

of the Atacama Desert, the proximity of the Altiplano (i.e., Andean Plateau) within the Central Andes Cordillera, and the need for better understanding of groundwater recharge processes to ultimately improve water resources management in the arid northern region. In the south of Chile, however, abundant surface water and groundwater resources coupled with remote locations have resulted in less frequent studies compared to the central and northern regions (Arumí and Oyarzún, 2006). Nevertheless, water-related stable isotope studies in the latter region are receiving increased attention (Hervé-Fernández et al., 2016; Lavergne et al., 2017).

A pioneering three-year data set (1984–1986) of precipitation isotopes from northern Chile by Aravena et al. (1999) showed $\delta^{18}\text{O}$ values ranging between -18‰ and -15‰ at high altitude stations, compared to -10‰ and -6‰ at lower elevations. The $\delta^{18}\text{O}$ -depleted values observed in the high altitude area, the Altiplano, were related to processes that affect the air masses that (i) originated over the Atlantic Ocean, (ii) cross the Amazon Basin (continental effect), (iii) ascended the Andes (altitude effect) and (iv) precipitated (convective effect) in the Altiplano. They also identified a second source of moisture, associated with air masses from the southeastern Pacific Ocean, which may have contributed to $\delta^{18}\text{O}$ -enriched values observed in lower altitude areas. Similar isotopic patterns were documented in springs and groundwater showing the representation of the long-term isotopic composition of rain in northern Chile. The relationship between the isotopic and chemical composition of rain, spring, and stream water in the high Andes of northern Chile was first studied by Fritz et al. (1981) and Magaritz et al. (1989). Fritz et al. (1981) reported that groundwater at Pampa del Tamarugal (within the Atacama Desert) originates from infiltrated surface water rather than directly infiltrated precipitation. Based on their low ^{14}C activities, the authors suggested that most of the water pumped was fossil. Magaritz et al. (1989) showed that the isotopic pattern of the springs in the high Andes of northern Chile is mainly a reflection of the altitude of their recharge areas, whereas processes that occur during snow melt seem to play a major role in the high-altitude springs. Similarly, the streams show analogous patterns to the springs in the higher part of the basins, but their isotopic composition is modified along the river course, mainly due to secondary evaporation processes along the river network. Hydrochemical studies in the Limarí River Basin in northern Chile (Oyarzún et al., 2014) showed an active interaction between surface water and shallow groundwater, and a minor effect of local precipitation events on the hydrological behavior in the study area. A recent study by Uribe et al. (2015) in closed basins within Salar del Huasco (northern Chile) estimated a long-term average recharge of 22 mm/yr and demonstrated no hydrogeological connectivity between the aquifer of the Salar del Huasco

Basin and the aquifer that feeds the springs of the nearby town of Pica. In central Chile, Ohlanders et al. (2013) determined glacier and snowmelt contributions to streamflow using stable isotopes in precipitation and surface water, whereby glacier and snowmelt inputs ranged from 50 up to 90% during dry La Niña years.

From a larger scale perspective, Bershaw et al. (2016) conducted an extensive study in modern surface water samples (including the northern Andean Plateau and surrounding regions) to elucidate patterns and causes of isotope fractionation in this continental environment. The authors reported a progressive increase in $\delta^{18}\text{O}$ of stream water west of the eastern Cordillera ($\sim 1\text{‰}/70\text{ km}$), which they attributed to a larger fraction of moisture recycling and a potential evaporative enrichment downwind, concluding that elevation is a primary control on the isotopic composition of surface water across the entire Andean Plateau and its surrounding areas. Consistent with the early findings by Aravena et al. (1999), Bershaw et al. (2016) and Fiorella et al. (2015a, b) suggested that precipitation patterns in the central Andes Cordillera are mainly governed by the easterly winds, which provide a large supply of moisture. The southeastern Pacific-derived moisture only contributes a minor amount at low elevations near the coast of, for example, La Serena. Similarly, Hoke et al. (2013) conducted a study on the eastern flank of the Andes in the Mendoza Province of Argentina, including a sampling transect in the western flank of the border with Chile (Las Cuevas, 3,200 m a.s.l.). Their results indicated that precipitation on the eastern slopes of the Andes at $\sim 33^\circ\text{ S}$, at elevations above 2 km, is largely derived from a westerly Pacific-source component and a mixture of easterly and westerly sources below 2 km.

The main goal of this chapter is to present a long-term analysis of water stable isotope ($\delta^{18}\text{O}$, $\delta^2\text{H}$, d -excess, and lc -excess) variations in precipitation across the extreme latitudinal and altitudinal gradients of Chile coupled with representative surface water, groundwater, geothermal and ice coring isotopic data. The core of temporal and spatial analysis is based on a 24-year (1991–2015) continuous record of monthly precipitation samples ($N = 684$) across four stations (from north to south): La Serena, Santiago, Puerto Montt and Punta Arenas. The isotopic values were obtained from the Isotopes Monitoring in Precipitation database of the Environmental Isotopes Laboratory of the Chilean Nuclear Energy Commission (GNIP-CCHEN) (<http://www.cchen.cl/>). Five discontinued short-term GNIP-CCHEN stations (1988–1991) were included for a better spatial coverage: Valparaíso, Temuco, Concepción, Chillán and Coyhaique. Additionally, representative precipitation, surface water, groundwater, geothermal and ice core isotopic data were obtained from the existing literature (Fritz et al., 1981; Aravena and Suzuki, 1990; Alpers and Whittemore, 1990; Aravena, 1995; Aravena

et al., 1999; Leybourne and Cameron, 2006; Ohlanders et al., 2013; Hoke et al., 2013; Oyarzún et al., 2014; Uribe et al., 2015; Fernández-Hervé et al., 2016) and from the isotopic archives of the International Atomic Energy Agency (IAEA, 2016). Long-term seasonal and temporal diagnostics are coupled with 10-day representative Lagrangian air mass back trajectories to highlight prevailing moisture sources and distinguish transport mechanisms as well as the influence of latitudinal isotopic effects during the wettest months. Analysis of these long-term water stable isotope data provides a fundamental baseline and revision for future isotope-informed modeling efforts and paleoclimate interpretations across the Pacific and Atlantic slopes within the southern Andes Cordillera biomes.

Climate Generalities

Chile is characterized by strong climatic gradients due to its unique geographical setting that extends over 4,000 km from around 18° S to almost 67° S (Fig. 9.57; Table 9.14). Such a longitudinal extension is coupled to an extreme topographical gradient from sea level up to ~ 6,900 m a.s.l. (i.e., Ojos del Salado volcano) with the Andes Cordillera traversing the continent and all of Chile. The Andes Cordillera act as an orographic barrier and separate Chile from air mass movements from the Atlantic Ocean (Aravena et al., 1999). Furthermore, Chile's climate is strongly influenced by the subtropical southeastern Pacific anticyclone (high pressure area) with cold sea currents (i.e., Humboldt Current) and low pressure systems forming off the Antarctic Sea (i.e., circumpolar low pressure area). Four main morphological units condition the existence of 11 different types of climate (from warm desert to polar/tundra) and associated vegetation: Coastal Plains, Coastal Mountains, Intermediate Depression and the Andes Cordillera (Smith and Evans, 2007).

As a consequence, northern Chile is characterized by the hyper-arid Atacama Desert with very low precipitation and high temperatures extending close to the city of La Serena (Verbist et al., 2010). According to the modified Köppen-Geiger climate classification by Peel et al. (2007), the area of La Serena is a cold desert climate (*BWk*) with annual rainfall of around 100 mm and a mean air temperature of 14°C (Fig. 9.57; Table 9.14). Peak rainfall occurs in winter (July) with virtually no rain during the summer months from November through April. Further to the south at an elevation of around 500 m a.s.l., the city of Santiago is characterized by a semi-arid cold steppe (*BSk*) climate with slightly higher annual precipitation of 329 mm on average and a mean annual air temperature of 13.9°C (Fig. 9.57; Table 9.14). Towards the central southern region of Chile rainfall is abundant with a mean annual amount of 1,952 mm at Puerto Montt and an average annual air temperature of 10.3°C (Fig. 9.57; Table 9.14).

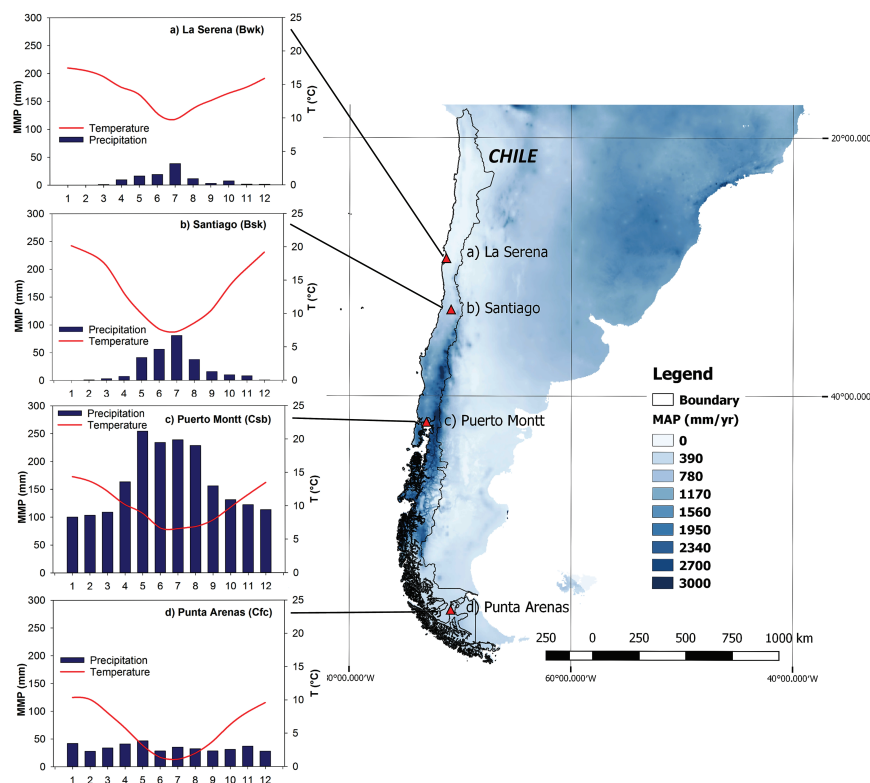


Fig. 9.57 Map of Chile including: long-term (24-years) stable isotope monitoring stations from GNIP-CCHEN (La Serena, Santiago, Puerto Montt and Punta Arenas) (red triangles), gridded mean annual precipitation (MAP) (mm yr^{-1}), and four climographs showing monthly mean precipitation (MMP) (blue bars) and monthly mean temperature (red line) for each station (both variables were derived from the most recent monthly gridded Global Historical Climatology Network, GHCN, version 3.0 product; Peterson and Vose, 1997). Based on the updated Köppen-Geiger world climate classification (Peel et al., 2007), the study site climates are classified as: mid-latitude cold desert (*BWk*, La Serena), semi-arid cold steppe (*Bsk*, Santiago), dry-summer or Mediterranean (*Csb*, Puerto Montt), and maritime temperate/sub-polar or oceanic (*Cfc*, Punta Arenas).

The climate of Puerto Montt is classified as dry-summer Mediterranean (*Csb*) with rainfall peaking in winter from June to September (Fig. 9.57; Table 9.14). In the Patagonia region, the climate of Punta Arenas can be described as maritime temperate (*Cfc*) with average annual rainfall of 410 mm and an average temperature of 5.8°C (Fig. 9.57; Table 9.14). Generally, precipitation increases with altitude and falls mostly as snow in the southern hemisphere winter, despite few high altitude measurements (Favier et al., 2009).

Table 9.14 Long-term (1991–2015) stable isotope characteristics in precipitation across Chile at four continuous monitoring stations.

Unit (‰)	La Serena (N = 40)			Santiago (N = 145)			Puerto Montt (N = 241)			Punta Arenas (N = 258)						
	$\delta^{18}\text{O}$	$\delta^2\text{H}$	d-ex	lc-ex	$\delta^{18}\text{O}$	$\delta^2\text{H}$	d-ex	lc-ex	$\delta^{18}\text{O}$	$\delta^2\text{H}$	d-ex	lc-ex	$\delta^{18}\text{O}$	$\delta^2\text{H}$	d-ex	lc-ex
Mean	-4.9	-29.6	9.8	1.7	-7.4	-50.6	8.3	-0.4	-5.5	-36.6	7.7	-0.5	-9.1	-70.5	2.3	-6.9
SD	2.2	15.9	5.5	11.6	2.7	21.3	5.1	17.5	2.7	18.7	5.8	18.8	3.3	23.8	6.9	11.7
Max	1.0	4.4	19.6	-11.7	-2.1	-3.0	25.1	-14.7	3.5	18.4	25.9	-19.8	3.5	18.4	19.2	-24.7
Min	-10.0	-76.0	-5.3	5.2	-13.7	-99.0	-6.3	5.0	-14.5	-101.1	-13.4	5.4	-21.4	-162.7	-17.7	6.5
w-mean	-5.6	-34.5	10.4	-0.2	-8.2	-55.0	10.9	1.7	-6.6	-43.1	9.7	0.6	-9.1	-72.1	0.6	-1.6

Methods

The 24-years (1991–2015) continuous record of monthly precipitation samples ($N = 684$) was compiled from data of four stations: La Serena (northern region, $\sim 30^\circ \text{S}$, 142 m a.s.l., $N = 40$), Santiago (inter-mountainous central region, $\sim 33^\circ \text{S}$, 520 m a.s.l., $N = 145$), Puerto Montt (southern coastal region, $\sim 41^\circ \text{S}$, 81 m a.s.l., $N = 241$) and Punta Arenas (Patagonia region, $\sim 53^\circ \text{S}$, 37 m a.s.l., $N = 258$) (Fig. 9.57). Monthly stable isotope archives ($\delta^{18}\text{O}$ and $\delta^2\text{H}$) of precipitation (1991–2015) were obtained from the GNIP-CCHEN (<http://www.cchen.cl/>) in cooperation with the Meteorological Directorate of Chile under the General Directorate of Civil Aviation of Chile (DGAC). The Chilean network is part of the GNIP initiative (GNIP-IAEA-WMO, 2016). This database also includes observed mean monthly air temperature ($^\circ\text{C}$) and monthly precipitation amount (mm). Mean monthly precipitation P (mm) and temperature T ($^\circ\text{C}$) characteristics were used to construct individual climographs (Fig. 9.57) were derived from the most recent monthly gridded Global Historical Climatology Network (GHCN) version 3.0 product (Peterson and Vose, 1997). In addition, gridded mean annual $\delta^{18}\text{O}$ (‰) in precipitation below $\sim 20^\circ \text{S}$ for South America was derived from Bowen and Revenaugh (2003) for comparison purposes.

Precipitation samples collected before 2009 were analyzed in a FINNIGAN Mat 252 Isotope Ratio Mass Spectrometer (IRMS) with an automatic equilibrium method ($\text{CO}_2\text{-H}_2\text{O}$; $\text{H}_2\text{-H}_2\text{O}$), the analytical precision was $\pm 0.2\text{‰}$ for $^{18}\text{O}/^{16}\text{O}$ and $\pm 1\text{‰}$ for $^2\text{H}/^1\text{H}$. After 2009, isotope compositions were measured by laser spectrometry using a LWIA-LGR DLT-100 (Los Gatos Research, USA) with an analytical precision of $\pm 0.08\text{‰}$ for $^{18}\text{O}/^{16}\text{O}$ and $\pm 1\text{‰}$ for $^2\text{H}/^1\text{H}$. Isotopic compositions were normalized to the VSMOW-SLAP scales, through the use of calibrated secondary laboratory standards and are defined as:

$$\delta^2\text{H}_{\text{sample}} = \frac{(^2\text{H}/^1\text{H})_{\text{sample}} - (^2\text{H}/^1\text{H})_{\text{VSMOW}}}{(^2\text{H}/^1\text{H})_{\text{VSMOW}}} \quad (1)$$

$$\delta^{18}\text{O}_{\text{sample}} = \frac{(^{18}\text{O}/^{16}\text{O})_{\text{sample}} - (^{18}\text{O}/^{16}\text{O})_{\text{VSMOW}}}{(^{18}\text{O}/^{16}\text{O})_{\text{VSMOW}}} \quad (2)$$

Deuterium excess (hereafter d -excess; Dansgaard, 1964) was calculated for each monthly sample (Equation 3). In addition, to determine the degree of deviation of monthly precipitation samples from regional/Local Meteoric Water Lines (LMWL), the line-conditioned excess (lc-excess) was calculated according to Landwehr and Coplen (2006) (Equation 4) (La Serena: $a = 6.97$, $b = 4.68$; Santiago: $a = 7.72$, $b = 6.64$; Puerto Montt: $a = 6.72$, $b = 0.63$; Punta Arenas: $a = 7.02$, $b = -6.62$). This calculation uses the LMWL as a reference rather than simply using the deviation from the GMWL (Sprenger et al.,

2017). The coefficients a and b are the slope and the y-intercept of the LMWL, respectively. Based on the analytical precision reported, the estimated average uncertainties are $\pm 1.1\text{‰}$ (d -excess) and $\pm 1.5\text{‰}$ (lc-excess).

$$d - excess = \delta^2H - 8 \cdot \delta^{18}O \quad (3)$$

$$lc - excess = \delta^2H - a \cdot \delta^{18}O - b \quad (4)$$

Five discontinued short-term GNIP-CCHEN stations (1988–1991) were included to achieve a better spatial coverage: Valparaíso (central coastal region, $\sim 33^\circ$ S, 41 m a.s.l., $N = 16$), Temuco (southern-central region, $\sim 39^\circ$ S, 114 m a.s.l., $N = 27$), Concepción (southern coastal region, $\sim 37^\circ$ S, 11 m a.s.l., $N = 19$), Chillán (southern-central region, $\sim 36^\circ$ S, 147 m a.s.l., $N = 27$) and Coyhaique (Patagonia region, $\sim 45^\circ$ S, 310 m a.s.l., $N = 117$) (Fig. 9.58). Additionally, representative precipitation, surface water, groundwater, geothermal and ice core isotopic data were obtained from the existing literature (Fritz et al., 1981; Aravena and Suzuki, 1990; Alpers and Whittemore, 1990; Aravena, 1995; Aravena et al., 1999; Leybourne and Cameron, 2006; Ohlanders et al., 2013; Hoke et al., 2013; Oyarzún et al., 2014; Uribe et al., 2015; Fernández-Hervé et al., 2016) and from the isotopic archives of IAEA (2016) (Fig. 9.58).

The influence of atmospheric trajectory and source meteorological conditions on the subsequent stable isotope composition of precipitation was analyzed using the HYSPLIT Lagrangian model (Stein et al., 2015) developed by the Air Resources Laboratory of NOAA (USA). The HYSPLIT model uses a three-dimensional Lagrangian air mass vertical velocity algorithm to determine the position of the air mass and reports these values at an hourly time-resolution over the trajectory (Soderberg et al., 2013). Representative 10-day air mass back trajectories were calculated for the three wettest months in 2015 at each monitoring station due to the nature of the monthly sampling. To compute a trajectory, the HYSPLIT model requires a starting time, location and altitude as well as NOAA meteorological data files (e.g., GDAS, global data assimilation system, 0.5° resolution: 2006-present; Su et al., 2015).

Results and Discussion

Regional isotopic characteristics

The best-fit continental meteoric water line to data from Chile (Chile-LMWL) is described as: $\delta^2H = 7.66 \cdot \delta^{18}O + 3.42$ ($r^2 = 0.94$, $N = 684$, $p < 0.001$) (Fig. 9.59A, top panel). Overall in the 24-years continuous record and across the four monitoring stations, $\delta^{18}O$ and δ^2H ranged from -21.4‰ to $+3.5\text{‰}$ and from -162.7‰ to $+18.4\text{‰}$, respectively (Figs. 9.59B and 9.59C, top panel), while d -excess ranged from -17.7‰ to $+25.9\text{‰}$

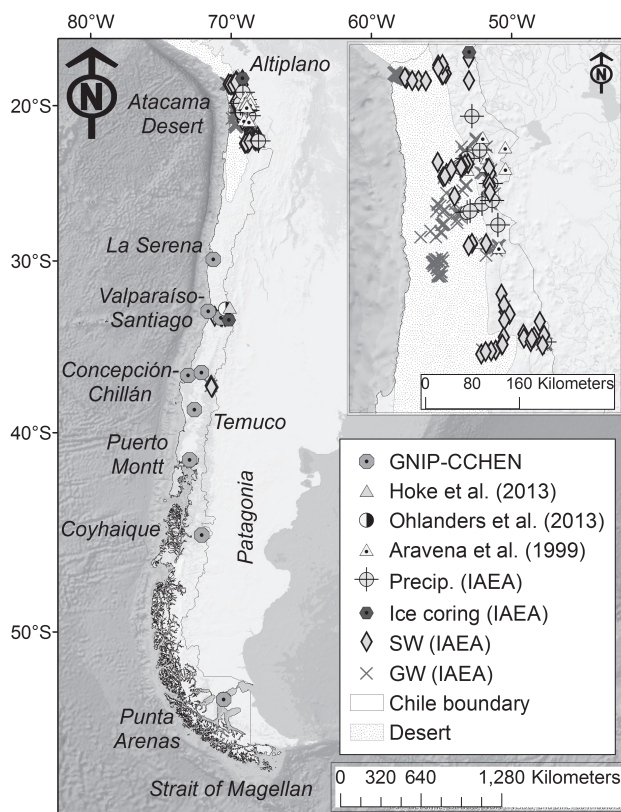


Fig. 9.58 Overview map of Chile including (a) the core GNIP-CCHEN monitoring stations and 5 discontinued short-term GNIP-CCHEN stations (pink octagons), (b) other precipitation samples from IAEA archives (green crossed-circles), (c) published precipitation data with available locations by Aravena et al. (1999) (yellow triangles), Hoke et al. (2013) (pink triangles), and Ohlanders et al. (2013) (yellow-black circles), (d) surface water (SW, cyan rhombi), groundwater (GW, blue crosses), and ice coring (red hexagons) isotope samples from IAEA archives. The inset shows the high concentration of isotopic sampling in northern Chile.

(mean = +7.0‰) and lc-excess varied from -6.9‰ to +1.7‰ (mean = -1.5‰) (Table 9.14). For the La Serena station, located near the southeastern Pacific coast (Fig. 9.57), the LMWL is described as: $\delta^2\text{H} = 6.97 \cdot \delta^{18}\text{O} + 4.68$ ($r^2 = 0.90$, $N = 40$, $p < 0.001$) (Fig. 9.59A, top panel). Since the northern region of Chile is semi-permanently under the influence of a high pressure system known as the sub-tropical southeastern Pacific anticyclone in combination with the cold Humboldt Current (Montecinos and Aceituno, 2003) and the isolation of the Atlantic Ocean moisture by the Andes Cordillera (Aravena et al., 1999), the precipitation events are less intense and occur mostly from May through August. Although the long-term d -excess at La

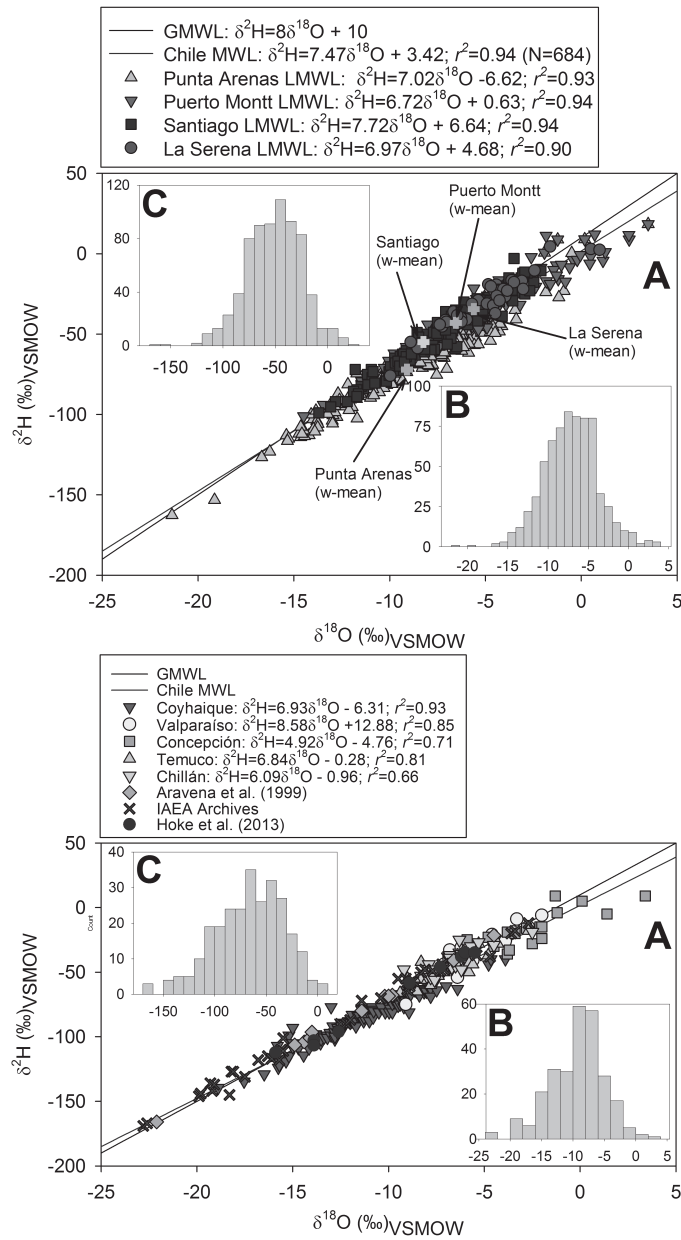


Fig. 9.59 Top panel: (A) Local Meteoric Water Lines (LMWLs) for each 24-years monitoring station. Bottom panel: (A) Local Meteoric Water Lines (LMWLs) for each discontinued short-term GNIP-CCHEN monitoring station and available data from Aravena et al. (1999), Hoke et al. (2013), and IAEA archives for Chile. The GMWL (black line) and Chile MWL (blue line) are plotted as references. Insets (B) and (C) in both panels show histograms for $\delta^{18}\text{O}$ (‰) and $\delta^2\text{H}$ (‰), respectively.

Serena (+9.8‰) is close to the global mean (+10‰; Craig, 1961), potential secondary evaporation processes below the cloud base during small rainfall events (MAP = 106 mm) coupled with a moderate mean annual air temperature range (10–20°C; Fig. 9.57) may introduce an artifact effect (Sánchez-Murillo et al., 2016a) which is responsible for the relatively lower slope and intercept values. For the Santiago station, located at a higher elevation (520 m a.s.l.) and approximately ~ 100 km from the Pacific coast, the LMWL is described as: $\delta^2\text{H} = 7.72 \cdot \delta^{18}\text{O} + 6.64$ ($r^2 = 0.94$, $N = 145$, $p < 0.001$) (Fig. 9.59A, top panel). Enhanced orographic distillation and greater precipitation amounts (MAP = 329; Fig. 9.57; Table 9.14) resulted in more depleted values with a mean $\delta^{18}\text{O}$ of -7.4‰ . In the southern coastal region of Puerto Montt, the LMWL can be described as $\delta^2\text{H} = 6.72 \cdot \delta^{18}\text{O} + 0.63$ ($r^2 = 0.94$, $N = 241$, $p < 0.001$) (Fig. 9.59A, top panel). This location experienced a typical temperate oceanic climate with large precipitation amounts year round (MAP = 1,952 mm; Fig. 9.57) and moderate mean annual air temperatures, ranging from 15°C down to 5°C. In the coastal Patagonia region of Punta Arenas, the LMWL is described as: $\delta^2\text{H} = 7.02 \cdot \delta^{18}\text{O} - 6.62$ ($r^2 = 0.93$, $N = 258$, $p < 0.001$) (Fig. 9.59A, top panel). Mean annual precipitation at Punta Arenas (410 mm) as well as mean annual temperature (ranging from 10°C down to 0°C) are considerably lower than at Puerto Montt (Fig. 9.57). In the last two locations, the lower intercepts may represent enhanced non-equilibrium processes due the influence of the circumpolar low pressure and temperature conditions from the Antarctic Sea. Overall, a clear latitudinal effect was observed in the isotopic composition along Chile. For instance, long-term *d*-excess and *lc*-excess exhibited a consistent decreasing latitudinal trend: +9.8‰ (+1.5‰) (La Serena), +8.3‰ (–0.4‰) (Santiago), +7.7‰ (–0.5‰) (Puerto Montt), and +2.3‰ (–6.9‰) (Punta Arenas) (Table 9.14), reflecting the influence of non-equilibrium processes as the mean annual temperature decreases towards the southern region, which favors snow formation and greater kinetic fractionation (Dansgaard, 1964). A similar decreasing trend was observed for $\delta^{18}\text{O}$ and $\delta^2\text{H}$ (Table 9.14).

For the five discontinued short-term (1988–1991) GNIP-CCHEN monitoring stations (Fig. 9.58), a similar isotopic pattern was observed when analyzing the LMWLs. For instance, the LMWL at Coyhaique (Patagonia region, Fig. 9.58) is described as: $\delta^2\text{H} = 6.93 \cdot \delta^{18}\text{O} - 6.31$ ($r^2 = 0.93$, $N = 117$, $p < 0.001$) (Fig. 9.59A, bottom panel) in concordance with the Punta Arenas-LMWL. The LMWLs at Temuco, Chillán, and Concepción (Fig. 9.58) also exhibited relatively low slopes (4.92 up to 6.84) and intercept (–4.76 up to –0.26) values (Fig. 9.59A, bottom panel). Valparaíso-LMWL is the only one across Chile from the GNIP-CCHEN database with a relatively high slope and intercept ($\delta^2\text{H} = 8.58 \cdot \delta^{18}\text{O} + 12.88$ ($r^2 = 0.85$, $N = 16$, $p < 0.001$)). However, the lower sample size may not be sufficient to establish further inferences. In general, the spectrum of isotopic composition in precipitation across Chile ranged from -22.8‰ up to $+3.5\text{‰}$ for $\delta^{18}\text{O}$ and from -169‰ up to $+18.4\text{‰}$

for $\delta^2\text{H}$ (Fig. 9.59B and 9.59C, in both panels). By combining all available isotopic precipitation records, the continental MWL can be described as: $\delta^2\text{H} = 7.59 \cdot \delta^{18}\text{O} + 3.25$ ($r^2 = 0.95$, $N = 957$, $p < 0.001$), which is quite similar to the one described by the 24-years continuous monitoring stations.

Long-term Spatial Variability

Dual relationships between $\delta^2\text{H}$, d -excess, and lc-excess (Figs. 9.66S; 9.67S) revealed a strong gradient from north to south and suggested a large influence of kinetic processes likely related to snow formation, particularly, in the southern region of Chile. In the arid region of La Serena, $\delta^{18}\text{O}$ and $\delta^2\text{H}$ ranged from -10.0‰ to $+1.0\text{‰}$ (mean = $-4.9 \pm 2.2\text{‰}$) and -76.0‰ to $+4.4\text{‰}$ (mean = $-29.6 \pm 15.9\text{‰}$), respectively. The values of d -excess and lc-excess ranged from $+19.6\text{‰}$ up to -5.3‰ (mean = $+9.8 \pm 5.5\text{‰}$) and from $+5.2\text{‰}$ up to -11.7‰ (mean = $+1.7 \pm 11.6\text{‰}$), respectively (Fig. 9.60a; Table 9.14). In the central region of Santiago, $\delta^{18}\text{O}$ and $\delta^2\text{H}$ ranged from -13.7‰ to -2.1‰ (mean = $-7.4 \pm 2.7\text{‰}$) and -99.0‰ to -3.0‰ (mean = $-50.6 \pm 21.3\text{‰}$), respectively, whereas d -excess and lc-excess fluctuated from $+25.1\text{‰}$ up to -6.3‰ (mean = $+8.3 \pm 5.1\text{‰}$) and from $+5.0\text{‰}$ up to -14.7‰ (mean = $-0.4 \pm 17.5\text{‰}$) (Fig. 9.60b; Table 9.14). In the southern coastal region of Puerto Montt, $\delta^{18}\text{O}$ and $\delta^2\text{H}$ ranged from -14.5‰ to $+3.5\text{‰}$ (mean = $-5.5 \pm 2.7\text{‰}$) and -101.1‰ to $+18.4\text{‰}$ (mean = $-36.6 \pm 18.4\text{‰}$), respectively. Likewise, d -excess and lc-excess varied from -13.4‰ up to $+25.9\text{‰}$ (mean = $+7.7 \pm 5.8\text{‰}$) and from $+5.4\text{‰}$ up to -19.8‰ (mean = $-0.5 \pm 18.8\text{‰}$) (Fig. 9.60c; Table 9.14). In Punta Arenas, $\delta^{18}\text{O}$ and $\delta^2\text{H}$ ranged from -21.4‰ to $+3.5\text{‰}$ (mean = $-9.1 \pm 3.3\text{‰}$) and -162.7‰ to $+18.4\text{‰}$ (mean = $-70.5 \pm 23.8\text{‰}$), respectively, whereas d -excess and lc-excess ranged from -17.7‰ up to $+19.2\text{‰}$ (mean = $+2.3 \pm 6.9\text{‰}$) and from $+6.5\text{‰}$ up to -24.7‰ (mean = $-6.9 \pm 11.7\text{‰}$) (Fig. 9.60d; Table 9.14).

Long-term Seasonal Variability

Long-term seasonality is well constrained across the four continuous monitoring stations (Fig. 9.57). Isotopic composition decreased from summer (DJF) to a minimum in winter (JJA) and increased again towards the spring season (SON) (Fig. 9.61; Table 9.15). In general, enriched and less variable isotopic values (-4.5‰ to -5.20‰ for $\delta^{18}\text{O}$ and -23.7‰ to -32.6‰ $\delta^2\text{H}$) were observed at La Serena (Fig. 9.61). This location is isolated from the influence of the Atlantic Ocean moisture by the central Andes Cordillera and received no rainfall in DJF. The most depleted values were observed at Punta Arenas monitoring station, where $\delta^{18}\text{O}$ composition decreased from -7.2‰ in summer (DJF) to -9.2‰ in autumn (MAM), reached a minimum of -10.7‰ in winter (JJA) and increased again to -9.1‰ in spring (SON).

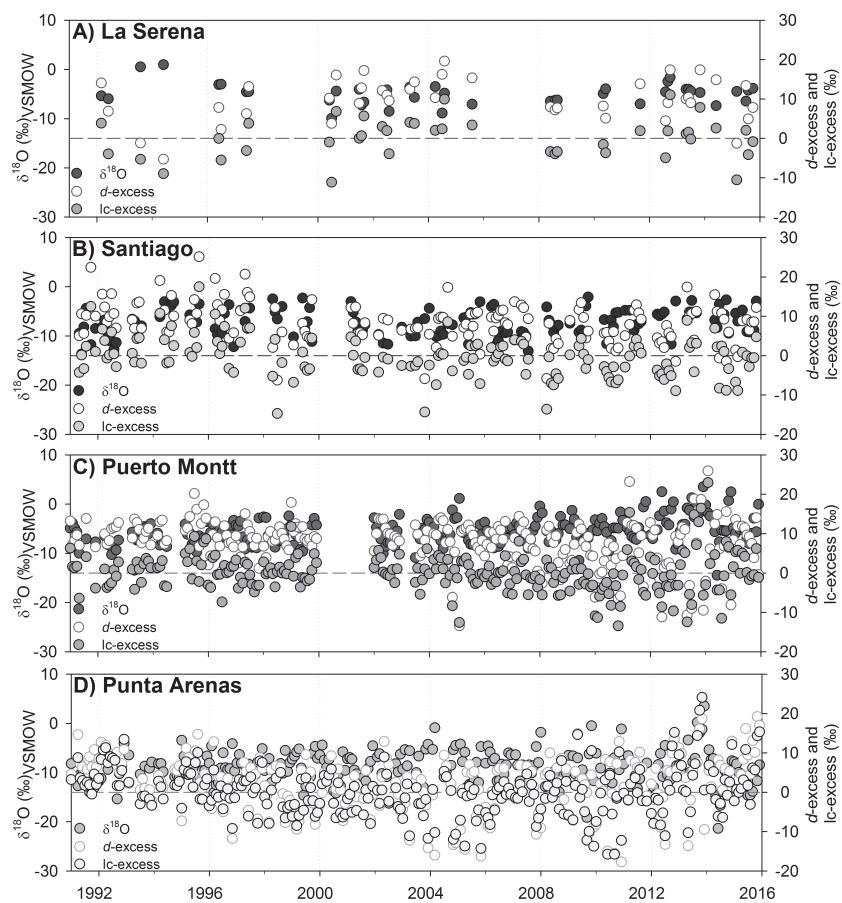


Fig. 9.60 Monthly $\delta^{18}\text{O}$ (‰), d -excess (‰), and lc -excess (‰) time series (1991–2015) of (A) La Serena, (B) Santiago, (C) Puerto Montt, and (D) Punta Arenas. Dashed-lines represent the lc -excess value of 0‰.

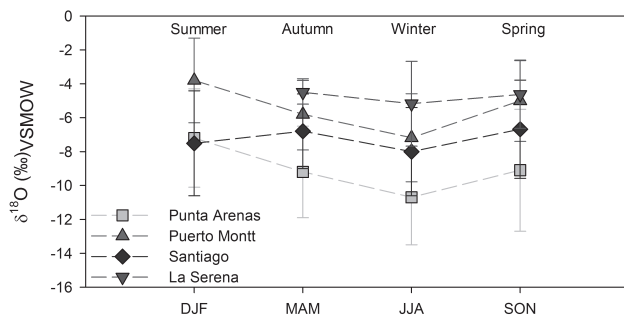


Fig. 9.61 Long-term seasonal $\delta^{18}\text{O}$ (‰) variability for each station. Seasons are grouped as: DJF (summer), MAM (autumn), JJA (winter), and SON (spring).

Table 9.15 Seasonal stable isotope characteristics in precipitation across Chile during 1991–2015.

Unit (%)	La Serena			Santiago			Puerto Montt			Punta Arenas		
	$\delta^{18}\text{O}$	$\delta^2\text{H}$	d-ex	$\delta^{18}\text{O}$	$\delta^2\text{H}$	d-ex	$\delta^{18}\text{O}$	$\delta^2\text{H}$	d-ex	$\delta^{18}\text{O}$	$\delta^2\text{H}$	d-ex
	Set-Oct-Nov (spring)											
Mean	-4.6	-23.7	13.3	-6.7	-45.4	8.0	-5.0	-33.2	6.8	-9.1	-70.6	2.3
SD	2.0	16.2	4.4	2.9	23.2	6.1	2.4	17.2	5.5	3.6	28.3	7.5
Max	-1.6	4.4	17.4	-2.1	-3.0	25.1	0.7	12.0	18.6	0.2	9.0	19.2
Min	-7.0	-42.5	7.7	-11.8	-88.9	-5.9	-9.3	-63.0	-9.6	-19.1	-153.2	-16.3
N	8	8	8	35	35	35	62	62	62	70	70	70
	Dec-Jan-Feb (summer)											
Mean	---	---	---	-7.5	-54.3	5.8	-3.8	-25.4	5.2	-7.2	-58.0	-0.4
SD	---	---	---	3.1	22.3	4.4	2.5	17.2	6.9	2.9	20.9	6.9
Max	---	---	---	-3.0	-25.1	13.7	3.5	18.4	25.9	3.5	18.4	17.0
Min	---	---	---	-12.2	-92.0	-1.5	-9.2	-64.4	-13.4	-14.5	-113.5	-17.7
N	---	---	---	10	10	10	52	52	52	60	60	60
	Mar-Apr-May (autumn)											
Mean	-4.5	-26.7	8.9	-6.8	-45.0	9.1	-5.8	-36.9	9.5	-9.2	-71.2	2.8
SD	0.7	7.1	5.4	2.2	17.3	5.7	2.1	15.1	4.8	2.7	17.7	6.9
Max	-3.5	-17.8	14.0	-2.5	-12.2	20.6	-0.8	-7.2	23.2	-0.9	-23.2	14.9
Min	-5.4	-37.2	-1.3	-11.5	-82.5	-5.9	-13.5	-94.0	-10.8	-14.7	-111.9	-16.0
N	6	6	6	35	35	35	62	62	62	64	64	64

	Jun-Jul-Aug (winter)													
Mean	-5.2	-32.6	8.8	-8.0	-55.4	8.4	-7.2	-48.6	8.9	-10.7	-81.6	4.3		
SD	2.5	17.1	5.6	2.6	21.1	4.2	2.6	17.6	5.4	2.8	21.0	5.3		
Max	1.0	2.8	19.6	-2.3	-10.4	16.0	2.5	8.8	20.2	-4.5	-46.0	16.1		
Min	-10.0	-76.0	-5.3	-13.7	-99.0	-6.3	-14.5	-101.1	-11.2	-21.4	-162.7	-15.0		
N	26	26	26	65	65	65	65	65	65	64	64	64		

Although, the seasonal pattern at Puerto Montt and Santiago followed the same trend, the isotopic composition at Santiago was more depleted due to its higher elevation and larger orographic distillation from the Pacific coast (~ 100 km), whereas at Puerto Montt, the isotopic composition is controlled mainly by the temperate maritime climate conditions (Fig. 9.61; Table 9.16).

Table 9.16 Mean monthly precipitation P (mm) and temperature T (°C) characteristics were derived from the most recent monthly gridded Global Historical Climatology Network (GHCN) version 3.0 product (Peterson and Vose, 1997). Total annual precipitation and annual average temperature are also given.

Month	La Serena		Santiago		Puerto Montt		Punta Arenas	
	P (mm)	T (°C)	P (mm)	T (°C)	P (mm)	T (°C)	P (mm)	T (°C)
January	0.0	17.5	10.0	21.0	238.7	6.6	35.2	1.1
February	0.0	17.5	10.0	20.0	228.5	6.8	32.2	2.0
March	1.0	16.5	12.0	18.0	155.9	7.8	28.2	3.8
April	9.4	15.0	16.0	15.0	130.9	9.6	30.7	6.3
May	16.2	13.5	52.0	12.0	121.9	11.6	36.7	8.2
June	18.9	12.0	42.0	9.0	113.1	13.4	27.6	9.6
July	38.2	12.0	86.0	9.0	100.1	14.3	41.9	10.4
August	11.4	12.0	45.0	10.0	103.3	13.6	27.8	10.1
September	3.0	13.0	24.0	12.0	108.9	12.1	33.6	8.1
October	7.1	14.0	12.0	15.0	163.3	10.1	41.0	5.8
November	1.3	15.0	10.0	17.0	254.1	8.9	46.6	3.2
December	0.8	16.5	10.0	19.0	233.8	6.7	28.2	1.4
Annual	106.0	14.0	329.0	13.9	1952.0	10.3	410.0	5.8

Summary of Isotopic Effects and Wider Implications

Despite the latitudinal difference, the Santiago station exhibited more depleted isotope values than Puerto Montt, most likely due to the orographic distillation in a ~ 100 km transect from the coast to approximately 520 m a.s.l. Nevertheless, the location of the four stations along a unique latitudinal transect (30° S–53° S) resulted in clear isotopic trends from north to south (Fig. 9.62). Overall, long-term $\delta^{18}\text{O}$ ($\delta^2\text{H}$) values ranged as follows: -4.9‰ (-29.6‰) (La Serena), -7.4‰ (-50.6‰) (Santiago), -5.5‰ (-36.6‰) (Puerto Montt) and -9.1‰ (-70.5‰) (Punta Arenas). Likewise, long-term d -excess and lc -excess exhibited a latitudinal decreasing trend: $+9.8\text{‰}$

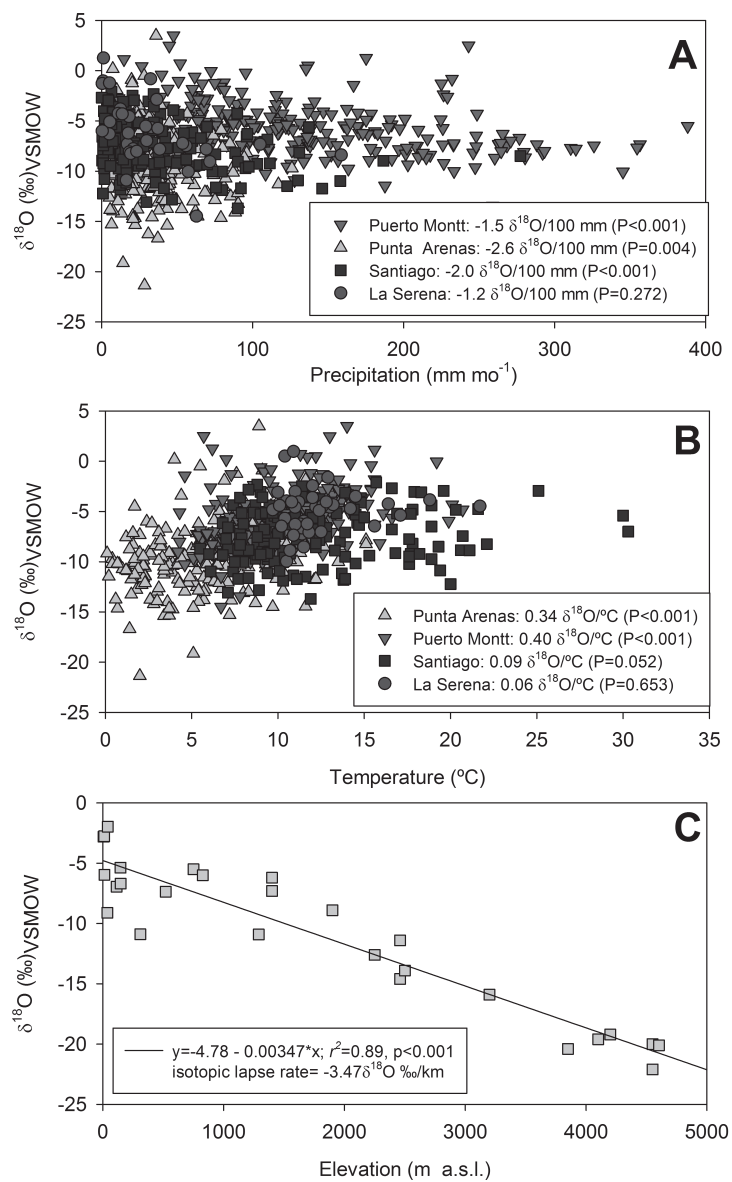


Fig. 9.62 (A) Monthly precipitation (mm) and $\delta^{18}\text{O}$ (‰) relationship for each station. (B) Air temperature ($^{\circ}\text{C}$) and $\delta^{18}\text{O}$ (‰) relationship for each station. (C) Elevation (m a.s.l.) and $\delta^{18}\text{O}$ (‰) relationship across Chile.

(+1.7‰) (La Serena) +8.3‰ (−0.4‰) (Santiago), +7.7‰ (−0.5‰) (Puerto Montt) and +2.3‰ (−6.9‰) (Punta Arenas), reflecting the influence of non-equilibrium processes as mean annual temperature decreases and snow formation increases towards the southern regions (Table 9.16). Normally, the latitudinal effect is in the order of $-0.6‰/\text{degree}$ and up to $-2‰/\text{degree}$ in the colder Antarctic continent (Mook, 2006). The latitudinal effect from La Serena (30° S , $\delta^{18}\text{O}$ mean = $-4.9‰$) and Punta Arenas (53° S , $\delta^{18}\text{O}$ mean = $-9.1‰$) was $\sim 0.2‰/\text{degree}$. The distinct monthly precipitation amounts converged in significant amount relationships at three locations: $-2.6‰/100\text{ mm}$ (Punta Arenas; $P = 0.004$), $-1.5‰/100\text{ mm}$ (Puerto Montt; $P < 0.001$) and $-2.0‰/100\text{ mm}$ (Santiago) for $\delta^{18}\text{O}$. Similar amount effects have been reported in high elevation cordilleras (up to 3,820 m a.s.l.; Sánchez-Murillo et al., 2016b). No significant precipitation amount relationship was found at La Serena station (Fig. 9.62A). A significant temperature effect was observed only at two stations: Punta Arenas ($+0.34‰/^\circ\text{C}$) and Puerto Montt ($+0.40‰/^\circ\text{C}$) $\delta^{18}\text{O}$, respectively (Fig. 9.62B). These values are in agreement with global temperature effects of $+0.4‰/^\circ\text{C}$ for $\delta^{18}\text{O}$ (Mook, 2006). However, Fiorella et al. (2015) conducted a precipitation collection in the central Andes Cordillera during 2008–2013 (elevation range: 395 to 4,340 m a.s.l.) and reported an isotopic lapse rate of $-1.9 \pm 0.5‰/\text{km}$. In addition, Poage and Chamberlain (2001) compiled 68 studies throughout many of the world's mountain belts and found an empirically consistent, linear relationship between change in elevation and change in the isotopic composition of precipitation along altitudinal transects. They concluded that there were no significant differences in isotopic lapse rates from most regions of the world ($\sim -2.8‰/\text{km}$). Figure 9.62C shows the relationship of $\delta^{18}\text{O}$ versus elevation (only for sites where elevations were properly reported). The elevation range covers $\sim 5,000\text{ m a.s.l.}$ Based on this significant linear regression, the orographic effect across the western slope of the southern Andes Cordillera can be described as $-3.47‰/\text{km}$ for $\delta^{18}\text{O}$ in contrast to an average lapse rate of $-1.45‰/\text{km}$ derived from Bowen and Revenaugh (2003).

The western slope of the Andes Cordillera is an exceptional case, because precipitation at higher elevation is controlled by continental air mass trajectories from the Atlantic Ocean, which travel through a wide range of biomes from the Amazon Basin to the Patagonia region, resulting in depleted precipitation. In contrast, in the coastal and central lowland regions, precipitation is mainly governed by the southeastern Pacific Ocean dynamics, resulting in enriched precipitation (Aravena et al., 1999). The combination of both processes is reflected in large apparent orographic effects, but also in remarkable spatial isotopic differences. Figure 9.63 shows a gridded mean annual $\delta^{18}\text{O}$ (‰) below $\sim 20^\circ\text{ S}$ for South America according to Bowen and Revenaugh (2003). Although, this

precipitation isoscape captures the isotopic difference within the western and eastern slopes of the Andes Cordillera, the relative magnitude of the isotopic composition appears to be strongly biased by the temperature effect, which is based solely on latitude and altitude estimations (e.g., $\delta^{18}O_p = a/Lat_x^2 + b/Lat_x + cAlt_x$; Bowen and Revenaugh, 2003), without taking into consideration the strong influence of the southeastern Pacific anticyclone (high pressure area) and circumpolar low pressure area from

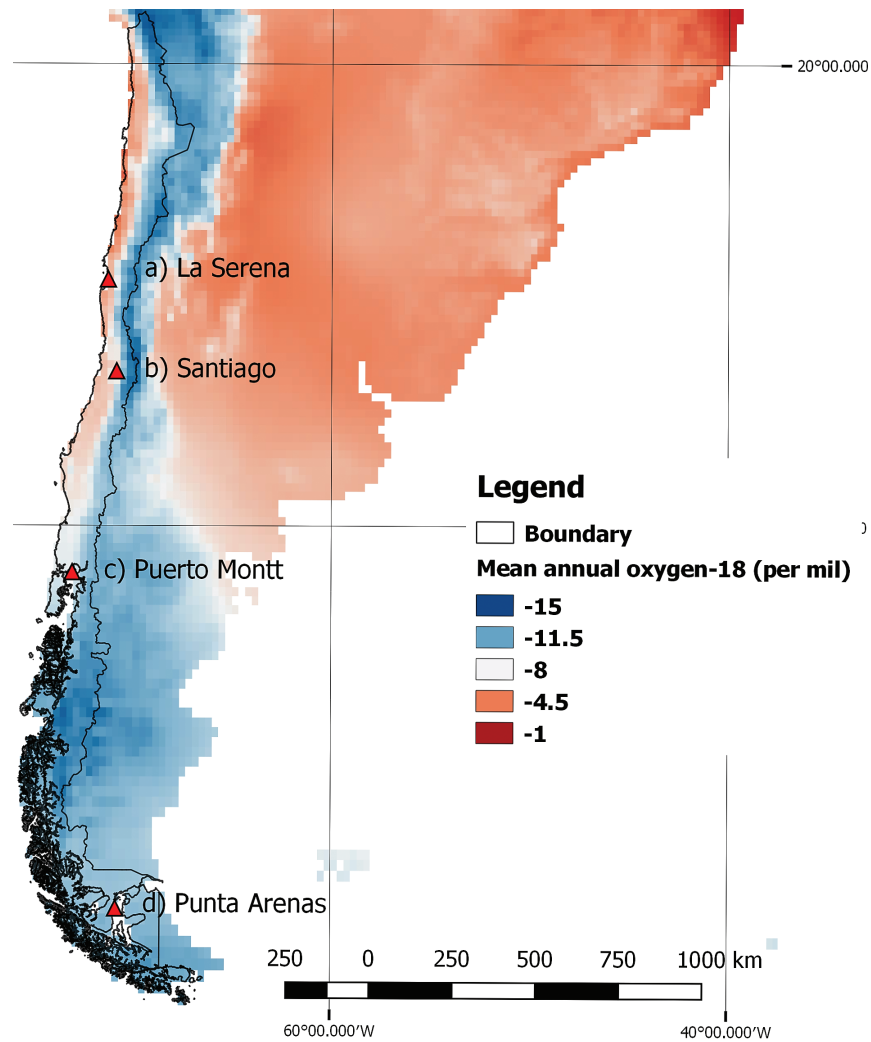


Fig. 9.63 Gridded mean annual $\delta^{18}O$ (‰) below $\sim 20^\circ S$ for South America according to Bowen and Revenaugh (2003). Long-term stable isotope monitoring stations are defined by red triangles.

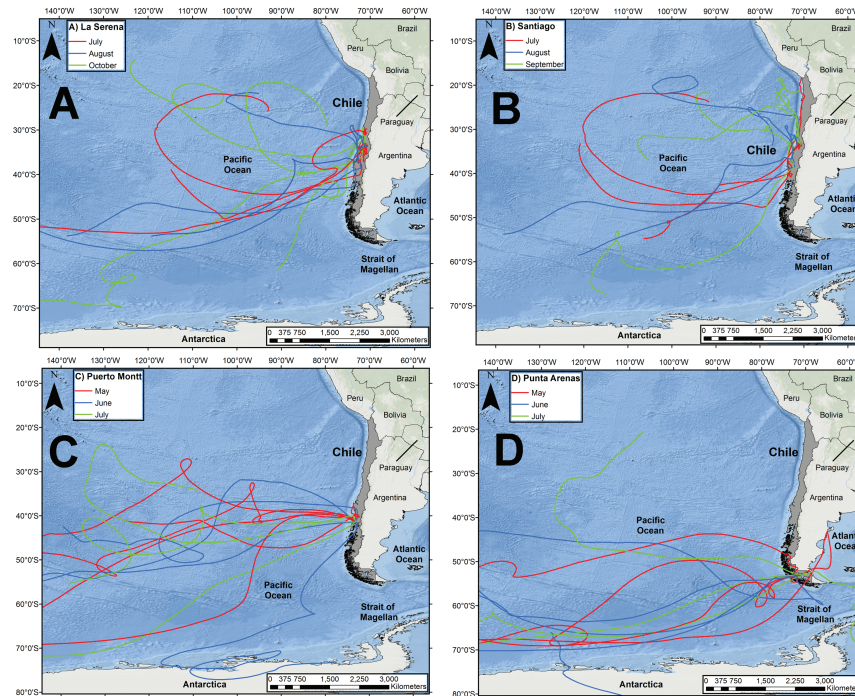


Fig. 9.64 Representative 10-day air mass back trajectories calculated using the HYSPLIT model (Stein et al., 2015) for the three wettest months in 2015 at La Serena (A), Santiago (B), Puerto Montt (C), and Punta Arenas (D) monitoring station. Months are color coded.

the Antarctic Sea. The latter is represented in the HYSPLIT air mass back trajectories (Fig. 9.64). During the wettest months, precipitation at La Serena and Santiago mainly originated from within the southeastern Pacific Ocean, whereas a strong Antarctic Sea influence was observed at Puerto Montt and Punta Arenas. Figure 9.65 shows representative isotopic data in different hydrological components. Although, historical isotopic studies in Chile have been highly concentrated in the northern region, the available data serve as a fundamental reference. As expected, ice coring data at high elevation sites presented the most depleted compositions but in a similar range of modern precipitation (Fig. 9.59). In the northern region, groundwater and surface water exhibited strong secondary evaporation processes; however, the isotopic spectrum (Fig. 9.65) also highlighted the relevance of spring recharge at high elevations in several locations in the western slope of the Andes Cordillera.

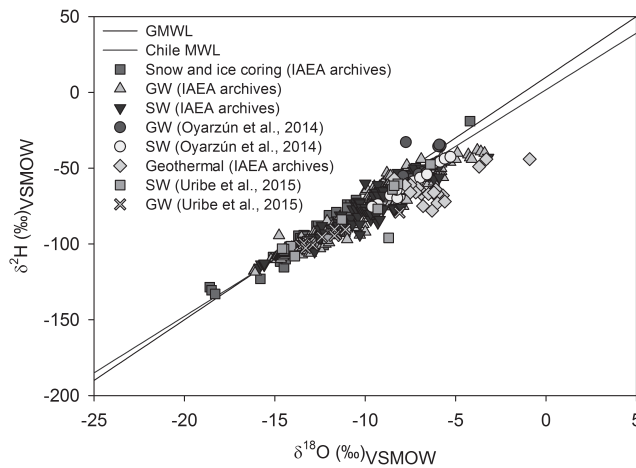


Fig. 9.65 Dual $\delta^2\text{H}$ – $\delta^{18}\text{O}$ (‰) diagram including: available isotopic data (i.e., surface water, groundwater, ice coring, and geothermal) from IAEA archives for Chile, Uribe et al. (2015), and Oyarzún et al. (2014). Samples are symbol and color coded.

Conclusions

Continuous (> 10-years) stable isotope records in precipitation along the Andes Cordillera are scarce. However, the recognition that modern precipitation dynamics may help to understand past climate conditions in paleo-archives has increased the number of monitoring efforts and related-hydrological studies. This study presents a long-term analysis (24-years) of monthly stable isotopes in precipitation across four stations in Chile (La Serena, Santiago, Puerto Montt and Punta Arenas). Overall, the 24-year continental meteoric water line of Chile is described as: $\delta^2\text{H} = 7.66 \delta^{18}\text{O} + 3.42$ ($r^2 = 0.94$) with a mean d -excess of $+7.0\text{‰}$. The second-order variables, d -excess (lc-excess), exhibited a strong latitudinal decreasing trend: $+9.8\text{‰}$ ($+1.5\text{‰}$) (La Serena), $+8.3\text{‰}$ (-0.4‰) (Santiago), $+7.7\text{‰}$ (-0.5‰) (Puerto Montt) and $+2.3\text{‰}$ (-6.9‰) (Punta Arenas), likely reflecting the influence of non-equilibrium processes as mean annual temperature decreases and snow formation is favored towards the southern regions. Long-term $\delta^{18}\text{O}$ ranged from enriched values within the northern semi-arid region of La Serena to a more depleted composition in the coastal Patagonia region of Punta Arenas, whereas intermediate $\delta^{18}\text{O}$ compositions were observed within the central and higher elevation region of Santiago and the southern coastal region of Puerto Montt. This isotopic pattern is well depicted in the surface water and groundwater domains.

Representative 10-day HYSPLIT air mass back trajectories revealed the strong influence of two major atmospheric transport mechanisms: the sub-tropical southeastern Pacific anticyclone (high pressure area) and the circumpolar low pressure area from the Antarctic Sea. The latitudinal spectrum among the monitoring network resulted in (a) a significant precipitation amount effect ($P < 0.01$) in three stations: -2.6‰ $\delta^{18}\text{O}/100$ mm (Punta Arenas), -1.5‰ $\delta^{18}\text{O}/100$ mm (Puerto Montt), and -2.0‰ $\delta^{18}\text{O}/100$ mm (Santiago), and (b) a temperature effect only significant ($P < 0.01$) at Punta Arenas ($+0.34\text{‰}$ $\delta^{18}\text{O}/^{\circ}\text{C}$) and Puerto Montt ($+0.40\text{‰}$ $\delta^{18}\text{O}/^{\circ}\text{C}$) stations. The relationship of $\delta^{18}\text{O}$ versus elevation (only for sites where elevations were properly reported) resulted in an orographic effect across the western slope of the southern Andes Cordillera of $-3.47\text{‰}/\text{km}$ for $\delta^{18}\text{O}$. Finally, the absence of a continuous sampling transect from the coast to the high elevations within the Andes Cordillera of Chile invokes the need of further investigation of altitude and/or orographic effects under a changing climate. This investigation should be complemented with the implementation of surface water and groundwater isoscapes, which can significantly improve the spatial understanding of hydrological connectivity between high elevation recharge and lowland discharge within the Pacific slope of the Andes Cordillera.

Acknowledgements

The authors would like to thank the support from the Environmental Isotopes Laboratory of the Chilean Nuclear Energy Commission (GNIP-CCHEN) (<http://www.cchen.cl/>) and the cooperation of the Meteorological Directorate of Chile belonging to General Directorate of Civil Aviation of Chile (DGAC). RS would like to recognize the support from the IAEA grant CRP-19747 under the initiative "Stable isotopes in precipitation and paleoclimatic archives in tropical areas to improve regional hydrological and climatic impact models" and the Research Office of the National University of Costa Rica through grants SIA-0482-13, SIA-0378-14, and SIA-0101-14. Similarly, the authors would like to thank the Water Resources Programme at the IAEA and the Nuclear Energy Commission of Chile for providing access to isotopic archives of Chile. CB was supported by the University of Costa Rica Research Council under project 237-B4-39. Support from the Isotope Network for Tropical Ecosystem Studies (ISONet) funded by the University of Costa Rica Research Council is also acknowledged.

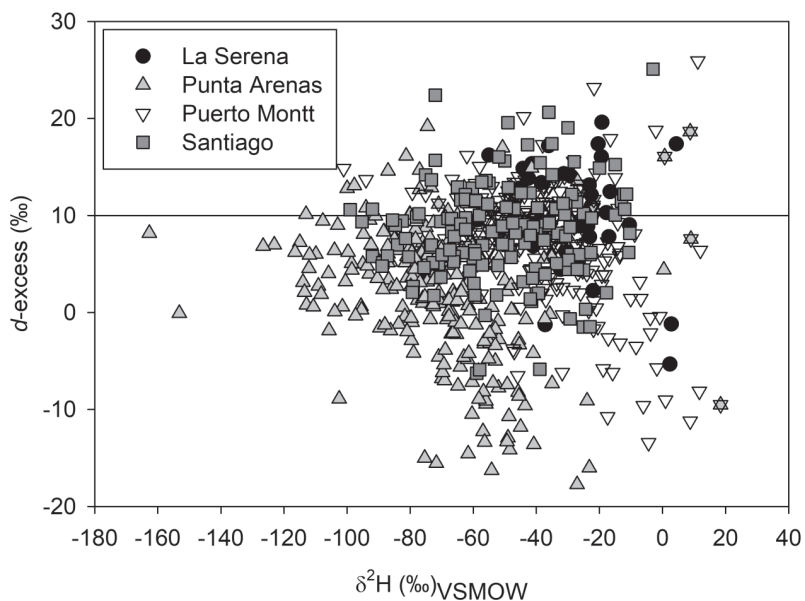


Fig. 9.66S $\delta^2\text{H}$ (‰) and $d\text{-excess}$ (‰) relationship for each long-term station. The horizontal black line denotes the $d\text{-excess}$ value of +10(‰).

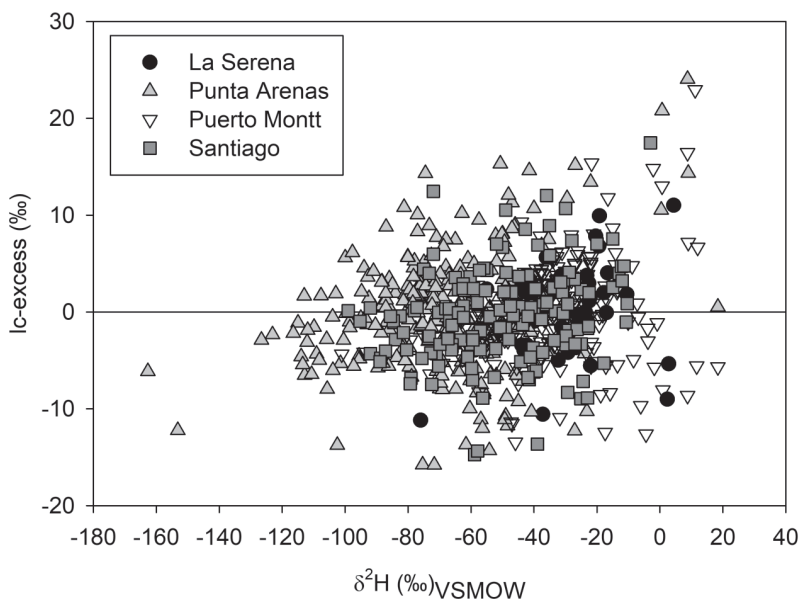


Fig. 9.67S $\delta^2\text{H}$ (‰) and $Ic\text{-excess}$ (‰) relationship for each long-term station. The horizontal black line denotes the $Ic\text{-excess}$ value of 0 (‰).

References

- Alpers, C.N. and Whittemore, D.O. 1990. Hydrogeochemistry and stable isotopes of ground and surface waters from two adjacent closed basins, Atacama Desert, northern Chile. *Applied Geochemistry* 5(5-6): 719–734. [http://dx.doi.org/10.1016/0883-2927\(90\)90067-F](http://dx.doi.org/10.1016/0883-2927(90)90067-F).
- Aravena, R. and Suzuki, O. 1990. Isotopic evolution of river water in the northern Chile region. *Water Resources Research* 26(12): 2887–2895. [http://dx.doi.org/10.1016/0168-9622\(89\)90008-0](http://dx.doi.org/10.1016/0168-9622(89)90008-0).
- Aravena, R. 1995. Isotope hydrology and geochemistry of northern Chile groundwaters. *Bull. IFEA* 24(3): 495–503.
- Aravena, R., Suzuki, O., Pena, H., Pollastri, A., Fuenzalida, H. and Grilli, A. 1999. Isotopic composition and origin of the precipitation in Northern Chile. *Applied Geochemistry* 14(4): 411–422. [http://dx.doi.org/10.1016/S0883-2927\(98\)00067-5](http://dx.doi.org/10.1016/S0883-2927(98)00067-5).
- Arumí Ribera, J.L. and Oyarzún Lucero, R.A. 2006. Groundwaters of Chile. *Boletín Geológico y Minero* 117(1): 37–45. Last accessed 2/1/2017. Available at: http://aprchile.cl/pdfs/LAs_aguas_subterraneeas_de_chile.PDF.
- Bershaw, J., Saylor, J.E., Garziona, C.N., Leier, A. and Sundell, K.E. 2016. Stable isotope variations ($\delta^{18}\text{O}$ and δD) in modern waters across the Andean Plateau. *Geochimica et Cosmochimica Acta* 194: 310–324. <http://dx.doi.org/10.1016/j.gca.2016.08.011>.
- Bowen, G. and Revenaugh, J. 2003. Interpolating the isotopic composition of modern meteoric precipitation. *Water Resour. Res.* 39: 1299. doi:10.1029/2003WR002086.
- Craig, H. 1961. Isotopic variations in meteoric waters. *Science* 133(3465): 1702–1703. Doi: 10.1126/science.133.3465.1702. <http://www.jstor.org/stable/1708089>.
- Dansgaard, W. 1964. Stable isotopes in precipitation. *Tellus* 16: 436–468. Doi: 10.1111/j.2153-3490.1964.tb00181.x.
- Favier, V., Falvey, M., Rabatel, A., Praderio, E. and López, D. 2009. Interpreting discrepancies between discharge and precipitation in high-altitude area of Chile's Norte Chico region (26–32° S). *Water Resources Research* 45: W02 424. Doi: 10.1029/2008WR006802.
- Fernández-Hervé, P., Oyarzún, C., Brumbt, C., Huygens, D., Bodé, S., Verhoest, N.E.C. and Boeckx, P. 2016. Assessing the 'two water worlds' hypothesis and water sources for native and exotic evergreen species in south-central Chile. *Hydrological Processes* 30(23): 4227–4241. Doi: 10.1002/hyp.10984.
- Fiorella, R.P., Poulsen, C.J., Zolá, R.S.P., Jeffery, M.L. and Ehlers, T.A. 2015a. Modern and long-term evaporation of central Andes surface waters suggests paleo archives underestimate Neogene elevations. *Earth and Planetary Science Letters* 432: 59–72. <http://dx.doi.org/10.1016/j.epsl.2015.09.045>.
- Fiorella, R.P., Poulsen, C.J., Pillco Zolá, R.S., Barnes, J.B., Tabor, C.R. and Ehlers, T.A. 2015b. Spatiotemporal variability of modern precipitation $\delta^{18}\text{O}$ in the central Andes and implications for paleoclimate and paleoaltimetry estimates. *J. Geophys. Res. Atmos.* 120: 4630–4656. Doi: 10.1002/2014JD022893.
- Fritz, P., Suzuki, O., Silva, C. and Salati, E. 1981. Isotope hydrology of groundwaters in the Pampa del Tamarugal, Chile. *Journal of Hydrology* 53(1-2): 161–184. [http://dx.doi.org/10.1016/0022-1694\(81\)90043-3](http://dx.doi.org/10.1016/0022-1694(81)90043-3).
- GNIP/IAEA/WMO. 2016. Global Network of Isotopes in Precipitation and Global Network of Isotopes in River. The GNIP and GNIR Databases. Accessible at: <http://www.iaea.org/water>. Last accessed: 21, December, 2016.
- Hoffmann, G., Ramirez, E., Taupin, J.D., Francou, B., Ribstein, P., Delmas, R., Dürr, H., Gallaire, R., Simões, J., Schotterer, U. and Stievenard, M. 2003. Coherent isotope history of Andean ice cores over the last century. *Geophysical Research Letters* 30(4). Doi: 10.1029/2002GL01487.
- Hoke, G.D., Aranibar, J.N., Viale, M., Araneo, D.C. and Llano, C. 2013. Seasonal moisture sources and the isotopic composition of precipitation, rivers, and carbonates across the

- Andes at 32.5–35.5° S. *Geochemistry, Geophysics, Geosystems* 14: 962–978. Doi: 10.1002/ggge.20045.
- Lavergne, A., Daux, V., Villalba, R., Pierre, M., Stievenard, M. and Srur, A.M. 2017. Improvement of isotope-based climate reconstructions in Patagonia through a better understanding of climate influences on isotopic fractionation in tree rings. *Earth and Planetary Science Letters* 459: 372–380. <http://dx.doi.org/10.1016/j.epsl.2016.11.045>.
- Leybourne, M.I. and Cameron, E.M. 2006. Composition of groundwaters associated with porphyry-Cu deposits, Atacama Desert, Chile: elemental and isotopic constraints on water sources and water–rock reactions. *Geochimica et Cosmochimica Acta* 70(7): 1616–1635. <http://dx.doi.org/10.1016/j.gca.2005.12.003>.
- Magaritz, M., Aravena, R., Peña, H., Suzuki, O. and Grilli, A. 1989. Water chemistry and isotope study of streams and springs in northern Chile. *Journal of Hydrology* 108: 323–341. [http://dx.doi.org/10.1016/0022-1694\(89\)90292-8](http://dx.doi.org/10.1016/0022-1694(89)90292-8).
- Montecinos, A. and Aceituno, P. 2003. Seasonality of the ENSO-related rainfall variability in central Chile and associated circulation anomalies. *Journal of Climate* 16(2): 281–96. [http://dx.doi.org/10.1175/1520-0442\(2003\)016<0281:SOTERR>2.0.CO;2](http://dx.doi.org/10.1175/1520-0442(2003)016<0281:SOTERR>2.0.CO;2).
- Mook, W.G. 2006. *Introduction to Isotope Hydrology*. Taylor & Francis. London, UK. 226 pp.
- Ohlanders, N., Rodriguez, M. and McPhee, J. 2013. Stable water isotope variation in a Central Andean watershed dominated by glacier and snowmelt. *Hydrology and Earth System Sciences* 17: 1035–1050. Doi: 10.5194/hess-17-1035-2013.
- Oyarzún, R., Barrera, F., Salazar, P., Maturana, H., Oyarzún, J., Aguirre, E., Alvarez, P., Jourde, H. and Kretschmer, N. 2014. Multi-method assessment of connectivity between surface water and shallow groundwater: the case of Limarí River basin, north-central Chile. *Hydrogeology Journal* 22: 1857–1873. Doi: 10.1007/s10040-014-1170-9.
- Oyarzún, R., Jofré, E., Morales, P., Maturana, H., Oyarzún, J., Kretschmer, N., Aguirre, E., Gallardo, P., Toro, L.E., Muñoz, J.F. and Aravena, R. 2015. A hydrogeochemistry and isotopic approach for the assessment of surface water–groundwater dynamics in an arid basin: the Limarí watershed, North-Central Chile. *Environmental Earth Sciences* 73(1): 39–55. Doi: 10.1007/s12665-014-3393-4.
- Oyarzún, R., Zambra, S., Maturana, H., Oyarzún, J., Aguirre, E. and Kretschmer, N. 2016. Chemical and isotopic assessment of surface water–shallow groundwater interaction in the arid Grande river basin, North-Central Chile. *Hydrological Sciences Journal* 61(12): 2193–2204. Doi: 10.1080/02626667.2015.1093635.
- Peel, M.C., Finlayson, B.L. and McMahon, T.A. 2007. Updated world map of the Köppen-Geiger climate classification. *Hydrol. Earth Syst. Sci.* 11: 1633–1644. Doi: 10.5194/hess-11-1633-2007, 2007.
- Perry, L.B., Seimon, A. and Kelly, G.M. 2014. Precipitation delivery in the tropical high Andes of southern Peru: new findings and paleoclimatic implications. *International Journal of Climatology* 34(1): 197–215. Doi: 10.1002/joc.3679.
- Peterson, T.C. and Vose, R.S. 1997. An overview of the global historical climatology network temperature database. *Bull. Am. Meteorol. Soc.* 78(12): 2837–2849.
- Poage, M.A. and Chamberlain, C.P. 2001. Empirical relationships between elevation and the stable isotope composition of precipitation and surface waters: considerations for studies of paleoelevation change. *American Journal of Science* 301(1): 1–15. Doi: 10.2475/ajs.301.1.1.
- Rozanski, K. and Araguás, L. 1995. Spatial and temporal variability of stable isotope composition over the South American continent. *Bulletin de l'Institut français d'études andines* 24(3): 379–390.
- Sánchez-Murillo, R., Birkel, C., Welsh, K., Esquivel-Hernández, G., Corrales-Salazar, J., Boll, J., Brooks, E.S., Roupsard, O., Sáenz-Rosales, O., Katchan, I. and Arce-Mesén, R. 2016a. Key drivers controlling stable isotope variations in daily precipitation of Costa Rica:

- Caribbean Sea versus Eastern Pacific Ocean moisture sources. *Quaternary Sci. Rev.* 131(Part B): 250–261. Doi: 10.1016/j.quascirev.2015.08.028.
- Sánchez-Murillo, R., Esquivel-Hernández, G., Sáenz-Rosales, O., Piedra-Marín, G., Fonseca-Sánchez, A., Madrigal-Solís, H., Ulloa-Chaverri, F., Rojas-Jiménez, L.D. and Vargas-Viquez, J.A. 2016b. Isotopic composition in precipitation and groundwater in the northern mountainous region of the Central Valley of Costa Rica. *Isotopes in Environmental and Health Studies*. Doi: 10.1080/10256016.2016.1193503.
- Schauwecker, S. 2011. Near-surface temperature lapse rates in a mountainous catchment in the Chilean Andes (Doctoral dissertation, Swiss Federal Institute of Technology Zurich).
- Smith, R.B. and Evans, J.P. 2007. Orographic precipitation and water vapor fractionation over the Southern Andes. *Journal of Hydrometeorology* 8: 3–19. Doi: 10.1175/JHM555.1.
- Sprenger, M., Tetzlaff, D., Tunaley, C., Dick, J. and Soulsby, C. 2017. Evaporation fractionation in a peatland drainage network affects stream water isotope composition. *Water Resources Research* 53. Doi: 10.1002/2016WR019258.
- Stein, A.F., Draxler, R.R., Rolph, G.D., Stunder, B.J.B., Cohen, M.D. and Ngan, F. 2015. NOAA's HYSPLIT atmospheric transport and dispersion modeling system. *Bulletin of the American Meteorological Society* 96: 2059–2077. Doi: 10.1175/BAMS-D-14-00110.1.
- Su, L., Yuan, Z., Fung, J.C.H. and Lau, A.K.H. 2015. A comparison of HYSPLIT backward trajectories generated from two GDAS datasets. *Science of the Total Environment* 506–507: 527–537. Doi: 10.1016/j.scitotenv.2014.11.072.
- Suzuki, O. and Aravena, R. 1990. Isotopic evolution of river water in the northern Chile region. *Water Resources Research* 26(12): 2887–2895.
- Uribe, J., Muñoz, J.F., Gironás, J., Oyarzún, R., Aguirre, E. and Aravena, R. 2015. Assessing groundwater recharge in an Andean closed basin using isotopic characterization and a rainfall-runoff model: Salar del Huasco basin, Chile. *Hydrogeology Journal* 23(7): 1535–1551. Doi: 10.1007/s10040-015-1300-z.
- Verbist, K., Robertson, A.W., Cornelis, W.M. and Gabriels, D. 2010. Seasonal predictability of daily rainfall characteristics in Central Northern Chile for dry-land management. *Journal of Applied Meteorology and Climatology* 49: 1938–1955. Doi: 10.1175/2010JAMC2372.1, 35 2010.
- Vimeux, F., Ginot, P., Schwikowski, M., Vuille, M., Hoffmann, G., Thompson, L.G. and Schotterer, U. 2009. Climate variability during the last 1000 years inferred from Andean ice cores: A review of methodology and recent results. *Palaeogeography, Palaeoclimatology, Palaeoecology* 281(3): 229–241. <http://dx.doi.org/10.1016/j.palaeo.2008.03.054>.
- Vuille, M., Bradley, R.S., Healy, R., Werner, M., Hardy, D.R., Thompson, L.G. and Keimig, F. 2003. Modeling $\delta^{18}\text{O}$ in precipitation over the tropical Americas: 2. Simulation of the stable isotope signal in Andean ice cores. *J. Geophys. Res.* 108: 4175. Doi: 10.1029/2001JD002039, D6.
- Wolfe, B.B., Aravena, R., Abbott, M.B., Seltzer, G.O. and Gibson, J.J. 2001. Reconstruction of paleohydrology and paleohumidity from oxygen isotope records in the Bolivian Andes. *Palaeogeography, Palaeoclimatology, Palaeoecology* 176(1): 177–192. [http://dx.doi.org/10.1016/S0031-0182\(01\)00337-6](http://dx.doi.org/10.1016/S0031-0182(01)00337-6).